RSC Advances

This is an *Accepted Manuscript*, which has been through the Royal Society of Chemistry peer review process and has been accepted for publication.

Accepted Manuscripts are published online shortly after acceptance, before technical editing, formatting and proof reading. Using this free service, authors can make their results available to the community, in citable form, before we publish the edited article. This *Accepted Manuscript* will be replaced by the edited, formatted and paginated article as soon as this is available.

You can find more information about *Accepted Manuscripts* in the Information for Authors.

Please note that technical editing may introduce minor changes to the text and/or graphics, which may alter content. The journal's standard Terms & Conditions and the Ethical guidelines still apply. In no event shall the Royal Society of Chemistry be held responsible for any errors or omissions in this *Accepted Manuscript* or any consequences arising from the use of any information it contains.

ROYAL SOCIETY OF CHEMISTRY

www.rsc.org/advances

RSC Advances

COMMUNICATION

Enhanced Efficiency of Planar-Heterojunction Perovskite Solar Cells through a Thermal Gradient Annealing Process

Received 00th January 20xx,
Accepted 00th January 20xx

DOI: 10.1039/x0xx00000x

www.rsc.org/

Bingbing Fan,[ab] Dehua Peng,[c] Shiwei Lin,[c] Nü Wang,[a] Yong Zhao,*[a] and Yanming Sun*[ab]

An efficient gradient annealing approach is demonstrated to improve the surface morphology and coverage of perovskite films. Gradient annealed perovskite films exhibit more uniform and smooth surface with improved coverage compared to directly annealed films. The resulting perovskite solar cells show enhanced device performance with a high efficiency of 14%, indicating that the gradient annealing process is a useful way to improve the efficiency of perovskite solar cells.

Organic-inorganic hybrid solar cells using halide lead perovskite materials as the photoactive layers have shown a rapid development in the past few years since the first organometal halide perovskite solar cells reported in 2009.[1] The power conversion efficiencies (PCEs) have been increased from 3.8% to 20.1% in just five years, revealing their great potential for future commercialization.[1-10] Perovskite solar cells utilizing mesoporous n-type metal oxide semiconductors (TiO_2, Al_2O_3, et. al) usually generate high PCEs.[3,6,11-13] For instance, efficiencies more than 18% have been recently reported for perovskite solar cells based on the rational incorporation of $MAPbBr_3$ into $FAPbI_3$ by using a mesoporous layer of TiO_2.[14] In addtion to the perovskite solar cells that combine a mesoporous electron transporting scaffold, planar heterojunction perovskite solar cells have recently attracted increasing attention due to their high efficiency and the low-temperature fabrication process.[15-19] Very recently, Im and co-workers have reported that a high PCE of 18.1% can be acheived for planar MAPbI3 perovskite hybrid solar cells with an inverted device architecture and the incorporation of dense pinhole-free $MAPbI_3$ as the light absorber.[20]

It has been realized now that the crystallinity and the surface coverage of perovskite films play significant roles in determing the performance of perovskite solar cells, which are critical to the charge transport and the stability of perovskite solar cells.[15,21,22] Efforts have been devoted to improving the crystallization and film coverage of the perovskite films. Numerous efficient approaches such as thermal/solvent annealing,[11,23,24] additive,[25-27] multi-step procedure[3,28-30] have been employed to control crystal growth and the film uniformity. Among the various approaches, thermal annealing has been employed to complete the conversion from the perovskite precursor into the perovskite film. The direct annealing (DA) at the temperature of, for example, 90 °C has been widely used to anneal the perovskite films.[31] In this contribution, we demonstrated that a gradient annealing process (GA) can be used to prepare the uniform perovskite films. In such a GA process, the perovskite film showed more uniform and smooth surface than the films directly annealed. The corresponding solar cells showed a high PCE of 14.0%, while the PCE of solar cells based on perovskite films with the DA process was 12.6%. The 11% improvement in efficiency is mainly ascribed to the improved perovskite film coverage, rather than the enhanced crystallization. This work paves the new way for improving the performance of organometal halide perovskite solar cells.

$CH_3NH_3PbX_3$ (X = Cl, I) perovskite materials have been reported to possess excellent photovoltaic property with high PCEs. The orthorhombic crystal structure of mixed-halide $CH_3NH_3PbI_{3-x}Cl_x$ was shown in Figure 1a, where blue spheres represent methylammonium cations, green spheres represent lead atoms, and purple spheres represent halide ions (I or Cl). The normalized UV-visible absorption spectra of the perovskite films prepared with the GA and DA processes were showed in Figure 1b. The perovskite films were prepared according to the following steps: firstly, the perovskite precursor solutions were spin cast on top of the ITO/poly(3,4-ethylene dioxythiophene):poly(styrene sulfonate)

[a] Key Laboratory of Bio-Inspired Smart Interfacial Science and Technology of Ministry of Education, Beijing Key Laboratory of Bio-inspired Energy Materials and Devices, School of Chemistry and Environment, Beihang University, Beijing 100191, PR China. E-mail: zhaoyong@buaa.edu.cn; sunym@buaa.edu.cn
[b] Heeger Beijing Research and Development Center, International Research Institute for Multidisciplinary Science, Beihang University, Beijing 100191, P. R. China.
[c] Key Laboratory of Ministry of Education for Advanced Materials in Tropical Island Resources, College of Materials and Chemical Engineering, Hainan University, Haikou 570228, P. R. China

† Electronic Supplementary Information (ESI) available: Schematic energy level diagram, device parameter (Jsc, Voc, FF and PCE) distribution. See DOI: 10.1039/x0xx00000x

RSC Advances Accepted Manuscript

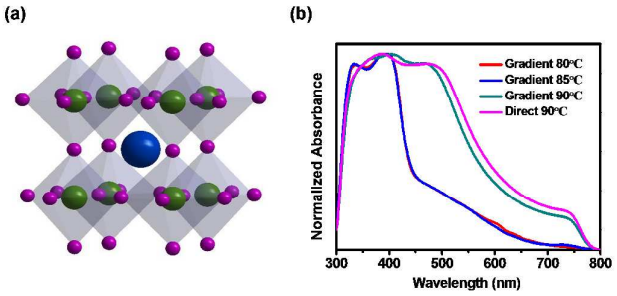

Figure 1. (a) Crystal structure of mixed halide perovskites with the formula of $CH_3NH_3PbI_{3-x}Cl_x$: blue color: organic groups $CH_3NH_3^+$; green color: Pb atom and purple color: halide atom (I or Cl). (b) UV-vis absorption spectra of $CH_3NH_3PbI_{3-x}Cl_x$ films with different annealing processes.

(PEDOT:PSS) substrates; then the films were treated via different thermal annealing processes. The total annealing time for the two processes is equal to 60 min. For samples with the GA process, the films were annealed at 80 °C for 20 min. Then, the temperature was increased steadily to 85 °C and the samples were annealed at this temperature for 20 min. After that, the temperature was further increased to 90 °C and the perovskite films were annealed for another 20 min. For the direct annealing process, the samples were annealed at 90 °C for 60 min. We noticed that the color of perovskite films was changed from bright yellow to dark brown after annealing at 90 °C. As shown in Figure 1b, there is low absorption in the wavelength range of 410-750 nm for perovskite films annealed at 80 °C and 85 °C, respectively. The absorption in this range was dramatically enhanced for perovskite films annealed at 90 °C, which confirmed the fact that the conversion process from the perovskite precursor into the $CH_3NH_3PbI_{3-x}Cl_x$ perovskite crystal upon annealing. In addition, we find that the perovskite films with the DA process show slightly red shift when compared to the perovskite films with the GA process, which probably comes from the difference in crystallization behavior for the films under different annealing conditions.

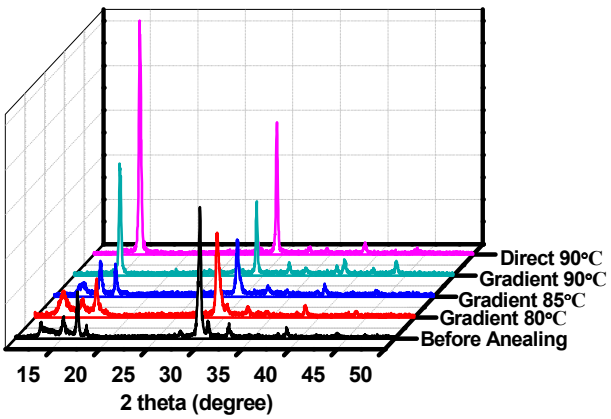

Figure 2. X-ray diffraction patterns of the evolving $CH_3NH_3PbI_{3-x}Cl_x$ films with different annealing processes.

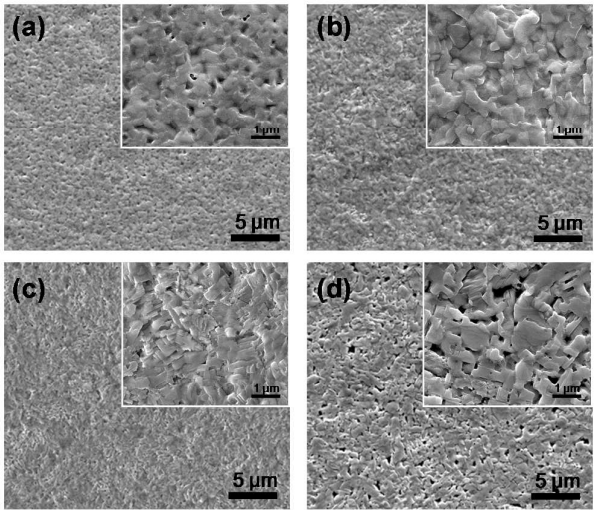

Figure 3. SEM images of the $CH_3NH_3PbI_{3-x}Cl_x$ films with the gradient annealing process. The films were annealed at 80 °C (a), 85 °C (b), and 90 °C (c) for 20 min. (d) SEM image of $CH_3NH_3PbI_{3-x}Cl_x$ films with the direct annealing process. The films were annealed at 90 °C for 60 min. The insets show the SEM images of the $CH_3NH_3PbI_{3-x}Cl_x$ films at different magnifications (scale bar, 1 μm).

The crystallization behavior of the resulting perovskite films was studied by using x-ray diffraction measurements (XRD). As shown in Figure 2, there are two main reflections located at 14.2° and 28.5°, corresponding to the (110) and (220) crystal planes of the orthorhombic lattice of mixed halide perovskites. The diffraction peaks at 14.2° increased significantly for perovskite films annealed at 90 °C, indicating the formation of perovskite crystal. When compared to the perovskite films with the GA process, perovskite films prepared through the DA process exhibited stronger reflections, suggesting the increased crystallization for the latter films.

Figure 3 showed the scanning electron microscope (SEM) images of the top topography of the evolving $CH_3NH_3PbI_{3-x}Cl_x$ films at different magnifications. In terms of the films annealed at 80 ºC, it shows that the perovskite precursors are randomly connected. Although the films look smooth, the perovskite materials are lacking the clear crystalline structure. As the annealing temperature increased to 85 °C, there is an obvious change in the appearance of the films. The films are composed of a lot of large perovskite domains. According to the XRD results, the annealing temperature at 85 °C is insufficient to lead to the formation of perovskite crystals. The large perovskite domains are still the perovskite precursor materials. When the annealing temperature was further increased to 90 °C, strip-like perovskite crystals were observed and the perovskite films are smooth and uniform with nearly 100% film coverage. The crystalline grain domains in perovskie films with the DA process were much larger than those prepared through the GA process. For the GA process, the annealing temperature was increased gradually from 80 ºC to 90 ºC, which can slow down the perovskite formation process, resulting in a better surface coverage. In contrast, the direct annealing at 90 ºC would accelerate the formation of perovskite crystal and create lots of

RSC Advances Accepted Manuscript

This journal is © The Royal Society of Chemistry 20xx

pinholes within the films, which will have negative influence on the charge transport and the stability of perovskite solar cells.

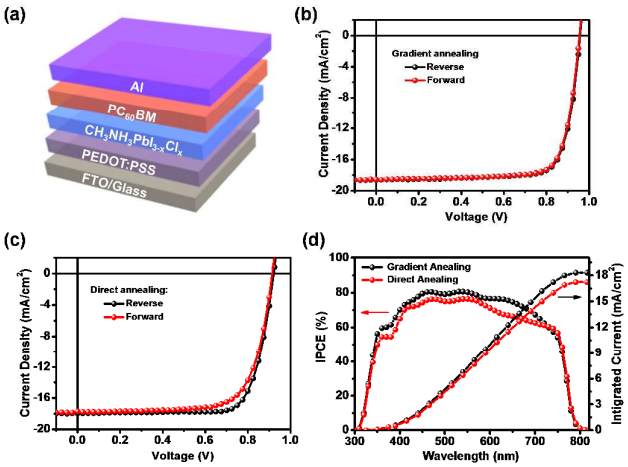

Figure 4. (a) Device structure of planar-heterojunction perovskite solar cells used in this study. J-V curves measured in the reverse and forward scanning directions for solar cells with the gradient annealing process (b) and the direct annealing process (c). (d) IPCE plots and the integrated current density of perovskite solar cells fabricated through different annealing processes.

Perovskite solar cells with the device architecture of FTO/PEDOT:PSS)/$CH_3NH_3PbI_{3-x}Cl_x$/phenyl-C_{60}-butyric acid methyl ester (PCBM)/Al were fabricated. The schematic energy diagram of each component in the device was shown in Figure S1. After the PCBM layer spin cast on top of the perovskite films and the deposition of the Al electrode, the perovskite solar cells were measured under the simulated AM 1.5G irradiation (100 mW/cm^2). Since the large photocurrent hysteresis was observed in many organometal trihalide perovskite solar cells and becomes a major issue in accurate characterization of the solar cell efficiency.[8,32,33] In this study, partial devices were measured with different scanning directions (reverse and forward scans) to measure the photocurrent hysteresis (Table 1 and S1). The current-voltage (J-V) characteristics of all solar cells were shown in Figure 4. The device parameters measured with forward and reverse sweep direction are summarized in Table 1.

Table 1. Device parameters of the perovskite solar cells fabricated with different annealing processes.

Annealing process	J_{sc} (mA/cm^2)	V_{oc} (V)	FF (%)	PCE (%)[a] average	PCE (%) best
Gradient	17.9±0.8	0.94±0.03	75 ± 4	12.6±1.4	14.0
Direct	16.9±1.2	0.89±0.03	75 ± 6	11.3±1.3	12.6

[a] The values are average efficiencies from 30 devices.

Perovskite solar cells fabricated with the GA process exhibited no photocurrent hysteresis when devices measured in the reverse and forward scanning directions, showing nearly the same PCEs (14.0% *vs.* 13.8%). For solar cells fabricated with the DA process, obvious photocurrent hysteresis was observed. The device measured in the reverse direction showed a PCE of 12.6% with short-circuit current (J_{sc}) of 17.9 mA/cm^2, open-circuit voltage (V_{oc}) of 0.92 V, and fill factor (FF) of 76.3%, while the cell measured in the forward direction exhibited a low PCE of 11.7%, mainly due to the decreased FF (72.3%). Recently, Huang and co-workers reported that the trap states on the surface and grain boundaries of the perovskite materials are the origin of photocurrent hysteresis in perovskite solar cells. [34] As shown in Figure 4d, the large grain boundaries and few pin holes may cause the photocurrent hysteresis. The incident photon conversion efficiency (IPCE) plots of solar cells are displayed in Figure 4d. The maximum IPCE value of devices with the GA and DA processes was nearly 80.0%. Obvious increases in IPCE in the wavelength range of 350-750 nm contributes to the increased J_{sc} of the devices fabricated with the GA process.

To further understand the performance differences between solar cells fabricated with the different annealing processes, more than 30 devices were fabricated in parallel for comparison. As shown in Table 1, the cells fabricated with the GA process showed an average PCE of 12.6% with J_{sc} of 17.9 mA/cm^2, and V_{oc} of 0.94 V, which are higher than devices with the DA process (Figure S2 and S3). The champion cell fabricated with the GA process showed a high PCE of 14%, with J_{sc} of 18.6 mA/cm^2, V_{oc} of 0.96 V, and FF of 78.3%. The J_{sc} calculated from IPCE spectrum was 18.3 mA/cm^2, which is in good agreement with the J_{sc} obtained from J-V curves (18.6 mA/cm^2) with a 1.7% mismatch. In the wavelength range of 400-750 nm, IPCE values are all higher than 60% with the maximum value of 80% at 470 nm, indicating high charge collection efficiency in cells.

The charge transport properties of perovskite layers were investigated by using space-charge-limited current (SCLC) method. The hole mobility was measured with the hole-only diode (FTO/PEDOT:PSS/$CH_3NH_3PbI_{3-x}Cl_x$/MoO_x/Al) (Figure S4). The hole mobility of perovskite films prepared via GA process is 1.8 ×10^{-2} cm^2/Vs, which is slightly higher than that (1.3 ×10^{-2}) of the perovskie films with the DA process, agreeing well with the higher J_{sc} value measured from I-V curves.

In conclusion, we demonstrated an efficient gradient annealing approach to improve the perovskite film coverage for low-temperature processed planar-heterojunction perovskite solar cells. The direct annealing process would accelerate the formation of perovskite crystal and create lots of pinholes within the films. The gradient annealing process can slow down the perovskite formation process, resulting in a better surface coverage. As a result, solar cells fabricated with the gradient annealing process show no photocurrent hysteresis with enhanced performance when compared to the cells with the direct annealing process. A high efficiency of 14% can be achieved, indicating that the gradient annealing process is a useful way to improve the efficiency of perovskite solar cells.

RSC Advances Accepted Manuscript

Experimental Section

Materials and Sample Preparation:

The methylammonium iodide (MAI) was synthesized by reaction with equimolar methylamine and hydriodic according to the previous reports.[2,26] MAI and $PbCl_2$ was mixed in anhydrous dimethylformamide (DMF) by a molar ratio of 3:1 with 1% 1,8-diiodooctane (DIO) to form the perovskite precursor solution (40 wt%). The mixture was stirred at 70 °C for overnight and kept at 90 °C with stirring for 15 min before use. The fluorine-doped tin oxide (FTO) coated glasses were ultrasonic cleaned in soapy water, deionized water, acetone, isopropanol, respectively, then dried overnight in a vacuum oven at 110 ºC and treated by UV-ozone for 30 min before use.

Device Fabrication and Characterization:

PEDOT:PSS was spin cast on top of FTO substrate at the speed of 4000 rpm for 40 s and dried at 145 °C for 10 min in air. Then, the substrate was transferred into nitrogen filled glove box. Perovskite precursor was spin cast atop the FTO/PEDOT:PSS substrate at 5000 rpm for 50 s. After exposure in N_2 atmosphere at room temperature for 10 min, the samples were placed onto a hotplate. For samples with the gradient annealing process, the films were annealed at 80 °C for 20 min, and the temperature was increased to 85 °C. The samples were annealed at this temperature for 20 min. After that, the temperature was further increased to 90 °C and the samples were annealed at 90 °C for another 20 min. For the direct annealing process, the samples were annealed at 90 °C for 60 min. After annealing at 90 °C, both samples turned to dark brown. Afterwards, PCBM layer was deposited onto the perovskite film from a chloroform solution (15 mg/ml) by spin coating at 1500~3500 rpm for 40 s. To complete the fabrication of device, a 100 nm-thick Al cathode was thermal evaporated onto the PCBM layer through a shadow mask (active area 4.5 mm^2) under a high vacuum pressure (6×10^{-5} Pa). During the measurement, an aperture with the area of 3.14 mm^2 was used to block stray light. Perovskite solar cells with GA and DA processes are measured under the same conditions. The devices were fabricated and measured all at N2 atmosphere in a glove box. The devices were measured with different scanning directions (reverse and forward scans). The scanning rate during the measurements is 25 mV/s and the delay time is 10 ms. Current density-voltage (J-V) curves were measured using a Keithley 2400 Source Measure Unit. Solar cell performance used an Air Mass 1.5 Global (AM 1.5 G) solar simulator (Class AAA solar simulator, Model 94063A, Oriel) with an irradiation intensity of 100 mW/cm^2, which was measured by a calibrated silicon solar cell and a readout meter (Model 91150V, Newport). IPCE spectra were measured by using a QEX10 Solar Cell IPCE measurement system (PV measurements, Inc.).

Film Characterization:

The SEM measurements were carried out on a Quanta 250 FEG SEM. The XRD measurements were recorded on. Shimadzu Lab-X XRD-6000 diffractometer with Cu Kα, λ = 1.54060 Å (the scan rate is 4°/min). UV-vis absorption measurements were carried out on a Shimadzu (model UV-3600) UV-vis spectrophotometer.

Acknowledgements

The authors acknowledge the 973 Program (2012CB933200), NSFC (21134003, 21222309, 21374001, 51462008), and the Fundamental Research Funds for the Central Universities for continuous financial support.

Notes and references

1 A. Kojima, K. Teshima, Y. Shirai, and T. Miyasaka, *J. Am. Chem. Soc.*, 2009, **131**, 6050-6051.
2 J. H. Im, C.R. Lee, J.W. Lee, S.W. Park, and N.G. Park, *Nanoscale*, 2011, **3**, 4088-4093.
3 J. Burschka, N. Pellet, S. J. Moon, R. Humphry-Baker, P. Gao, M. K. Nazeeruddin, and M. Gratzel, *Nature*, 2013, **499**, 316-319.
4 S. D. Stranks, G. E. Eperon, G. Grancini, C. Menelaou, M. J. Alcocer, T. Leijtens, L. M. Herz, A. Petrozza, and H. J. Snaith, *Science*, 2013, **342**, 341-344.
5 H. S. Kim, C.R. Lee, J. H. Im, K. B. Lee, T. Moehl, A. Marchioro, S. J. Moon, R. Humphry-Baker, J. H. Yum, J. E. Moser, M. Gratzel, and N. G. Park, *Sci. Rep.*, 2012, **2**, 591.
6 M. M. Lee, J. Teuscher, T. Miyasaka, T. N. Murakami, and H. J. Snaith, *Science*, 2012, **338**, 643-647.
7 A. Mei, X. Li, L. Liu, Z. Ku, T. Liu, Y. Rong, M. Xu, M. Hu, J. Chen, Y. Yang, M. Gratzel, and H. Han, *Science*, 2014, **345**, 295-298.
8 N. J. Jeon, J. H. Noh, Y. C. Kim, W. S. Yang, S. Ryu, and S. I. Seok, *Nat. Mater.*, 2014, **13**, 897-903.
9 H. Zhou, Q. Chen, G. Li, S. Luo, T.B. Song, H.S. Duan, Z. Hong, J. You, Y. Liu, and Y. Yang, *Science*, 2014, **345**, 542-546.
10 NREL, In http://www.nrel.gov/ncpv/.
11 L. Etgar, P. Gao, Z. Xue, Q. Peng, A. K. Chandiran, B. Liu, M. K. Nazeeruddin, and M. Gratzel, *J. Am. Chem. Soc.*, 2012, **134**, 17396-17399.
12 J. M. Ball, M. M. Lee, A. Hey, and H. J. Snaith, *Energy Environ. Sci.*, 2013, **6**, 1739.
13 W. Zhang, M. Saliba, S. D. Stranks, Y. Sun, X. Shi, U. Wiesner, and H. J. Snaith, *Nano Lett.*, 2013, **13**, 4505-4510.
14 N. J. Jeon, J. H. Noh, W. S. Yang, Y. C. Kim, S. Ryu, J. Seo, and S. I. Seok, *Nature*, 2015, **517**, 476-480.
15 J. Y. Jeng, Y. F. Chiang, M. H. Lee, S. R. Peng, T. F. Guo, P. Chen, and T. C. Wen, *Adv. Mater.*, 2013, **25**, 3727-3732.
16 M. Liu, M. B. Johnston, and H. J. Snaith, *Nature*, 2013, **501**, 395-398.
17 Q. Chen, H. Zhou, Z. Hong, S. Luo, H. S. Duan, H. H. Wang, Y. Liu, G. Li, and Y. Yang, *J. Am. Chem. Soc.*, 2014, **136**, 622-625.
18 D. Liu and T. L. Kelly, *Nat. Photonics*, 2013, **8**, 133-138.
19 W. Wang, J. Yuan, G. Shi, X. Zhu, S. Shi, Z. Liu, L. Han, H. Q. Wang, and W. Ma, *ACS Appl. Mater. Interfaces*, 2015, **7**, 3994-3999.
20 J. H. Heo, H. J. Han, D. Kim, T. K. Ahn, and S. H. Im, *Energy Environ. Sci.*, 2015, **8**, 1602-1608.
21 B. Conings, L. Baeten, C. De Dobbelaere, J. D'Haen, J. Manca, and H. G. Boyen, *Adv. Mater.*, 2014, **26**, 2041-2046.
22 P. Docampo, J. M. Ball, M. Darwich, G. E. Eperon, and H. J. Snaith, *Nat. Commun.*, 2013, **4**, 2761.
23 H. L. Hsu, C. P. Chen, J. Y. Chang, Y. Y. Yu, and Y. K. Shen, *Nanoscale*, 2014, **6**, 10281-10288.
24 Z. Xiao, Q. Dong, C. Bi, Y. Shao, Y. Yuan, and J. Huang, *Adv. Mater.*, 2014, **26**, 6503-6509.
25 C. Y. Chang, C. Y. Chu, Y. C. Huang, C. W. Huang, S. Y. Chang, C. A. Chen, C. Y. Chao, and W. F. Su, *ACS Appl. Mater. Interfaces*, 2015, **7**, 4955-4961.
26 P. W. Liang, C. Y. Liao, C. C. Chueh, F. Zuo, S. T. Williams, X. K. Xin, J. Lin, and A. K. Jen, *Adv. Mater.*, 2014, **26**, 3748-3754.
27 C. Zuo and L. Ding, *Nanoscale*, 2014, **6**, 9935-9938.
28 Y. Chen, T. Chen, and L. Dai, *Adv. Mater.*, 2015, **27**, 1053-1059.
29 Z. Xiao, C. Bi, Y. Shao, Q. Dong, Q. Wang, Y. Yuan, C. Wang, Y. Gao, and J. Huang, *Energy Environ. Sci.*, 2014, **7**, 2619.

RSC Advances Accepted Manuscript

This journal is © The Royal Society of Chemistry 20xx

30 F. Hao, C. C. Stoumpos, Z. Liu, R. P. Chang, and M. G. Kanatzidis, *J. Am. Chem. Soc.*, 2014, **136**, 16411–16419.
31 J. H. Kim, S. T. Williams, N. Cho, C.-C. Chueh, and A. K. Y. Jen, *Adv. Energy Mater.*, 2015, **5**, 1401229.
32 H. J. Snaith, A. Abate, J. M. Ball, G. E. Eperon, T. Leijtens, N. K. Noel, S. D. Stranks, J. T.-W. Wang, K. Wojciechowski, and W. Zhang, *J. Phys. Chem. Lett*, 2014, **5**, 1511-1515.
33 L. K. Ono, S. R. Raga, S. Wang, Y. Kato, and Y. Qi, *J. Mater. Chem. A*, 2015, **3**, 9074-9080.
34 Y. Shao, Z. Xiao, C. Bi, Y. Yuan, and J. Huang, *Nat. Commun.*, 2014, **5**, 5784.

RSC Advances Accepted Manuscript

Table of Contents Entry

An efficient gradient annealing approach has been developed to improve the surface morphology and coverage of perovskite films, thereby increasing the efficiency of perovskite solar cells.

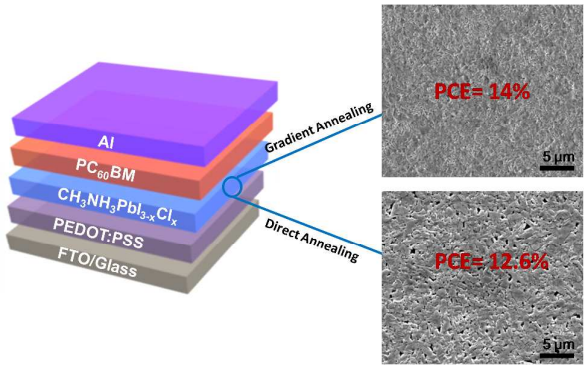

RSC Advances Accepted Manuscript